added and the mixture was stirred at −78 °C for 4 h and slowly warmed to 20 °C. The reaction mixture was then poured into saturated aqueous ammonium chloride and THF was evaporated under reduced pressure. The residue was extracted three times with ethyl acetate (150 mL × 3). The combined organic phases were washed with brine, dried over sodium sulfate, filtered, and concentrated in vacuo. The residual oil was purified by flash chromatography using petroleum ether and increasing amounts of ethyl acetate as eluents to give **5** (17.7 g, 40%) as a pale yellow oil ^{1}H NMR ($CDCl_3$) δ 4.30 (m, 4 H), 3.25 (t, 2 H), 1.65–2.4 (m, 6 H), 1.40 (t, 6 H); ^{19}F NMR ($CDCl_3$, C_6H_6 as reference) δ 51 (dt, J_{H-F} = 21 Hz, J_{F-P} = 112 Hz); MS (CI, NH_3) *m/z* 388 (MNH_4^+), 371 (MH^+), 262.

2-Amino-6-chloro-9-[5,5-difluoro-5-(diethylphosphono)pentyl]purine (6). Anhydrous potassium carbonate (66 mmol, 9.1 g) was added to a stirred suspension of 2-amino-6-chloropurine (6.1 g, 36 mmol) and 5-iodo-1,1-difluoro-1-(diethylphosphono)pentane (**5**; 12.2 g, 33 mmol) in 65 mL of anhydrous DMF at 20 °C under argon. The reaction mixture was stirred at 20 °C for 22 h, filtered over Celite, and evaporated under reduced pressure. The crude residue was purified by flash chromatography on silica gel using ethyl acetate as eluent to give **6** (8.4 g, 62%: ^{1}H NMR (CD_3OD) δ 8.1 (s, H_8), 4.9 (s, NH_2), 4.25 (m, 4 H), 4.15 (t, CH_2N), 2.15 (m, CH_2CF_2), 1.95 (m, CH_2), 1.55 (m, CH_2), 1.3 (t, 6 H, OCH_2CH_3); ^{19}F NMR (CD_3OD; C_6F_6 as reference) δ 52.5 (dt, J_{F-H} = 19 Hz, J_{F-P} = 111 Hz); MS (CI, NH_3) *m/z* 412 (MH^+). Anal. Calcd for $C_{14}H_2N_5ClF_2PO_3$: C, 40.83; H, 5.14; N, 17.00. Found: C, 40.46; H, 5.21; N, 16.97.

9-(5,5-Difluoro-5-phosphonopentyl)guanine (3). Bromotrimethylsilane (9 g, 59 mmol) was added dropwise to a stirred solution of **6** (6 g, 14.6 mmol) in 80 mL of anhydrous dichloromethane at 20 °C under argon. The reaction mixture was stirred at 20 °C for 44 h and evaporated under reduced pressure. The residue was dissolved in anhydrous acetonitrile, and a pale yellow precipitate was obtained upon addition of 1 mL of water. The solid was collected by filtration giving 5.4 g of product, which was suspended in 50 mL of 1 N HCl and heated at 95 °C for 18 h. The reaction mixture was evaporated under reduced pressure; the residue obtained was dissolved in boiling water and crystallized on cooling, giving 4.6 g of **3** (93% yield from **6**): mp 260 °C; TLC, R_f = 0.44 (EtOH/17% NH_4OH, 60/40); ^{1}H NMR (D_2O, NaOD) δ 8.3 (s, H_8), 4.2 (t, CH_2N), 2.15 (m, CH_2CF_2), 1.95 (m, CH_2), 1.65 (m, CH_2); ^{19}F NMR (D_2O, NaOD, CF_3CO_2H as reference) δ −36.6 (dt, J_{F-P} = 97 Hz, J_{H-F} = 20 Hz); MS (FAB, xenon) *m/z* 338 (MH^+), 185. Anal. Calcd for $C_{10}H_{14}F_2N_5O_4P{\cdot}HCl$: C, 32.14; H, 4.04; N, 18.74. Found: C, 31.75; H, 4.39; N, 18.32.

9-(7,7-Difluoro-7-phosphonoheptyl)guanine (7). 9-(7,7-Difluoro-7-phosphonoheptyl)guanine was obtained from diethyl difluoromethanephosphonate, 1,6-diiodohexane, and 6-chloroguanine according to the procedure described for the preparation of **3**. However, in this case, the final product was obtained in a pure form by recrystallization in a 1 M water solution of triethylammonium bicarbonate. **7**: mp 280 °C; TLC, R_f = 0.49 (ETOH/17% NH_4OH, 60/40); ^{1}H NMR (D_2O, NaOD) δ 7.8 (s, H_8), 4.05 (t, CH_2N), 2.03 (m, CH_2CF_2), 1.75 (m, CH_2), 1.45 (m, CH_2), 1.3 (m, 2 CH_2); ^{19}F NMR (D_2O, NaOD, $CF_3CO_2^-$ as reference) δ −36.6 (dt, J_{H-F} = 21 Hz, J_{F-P} = 89 Hz); MS (FAB, xenon) *m/z* 366 (MH^+). Anal. Calcd for $C_{12}H_{18}F_2N_5O_4P$: C, 39.46; H, 4.97; N, 19.17. Found: C, 39.36; H, 5.08; N, 18.64.

Enzymes and Assays. PNP from human erythrocytes, calf spleen, and *E. coli* were purchased from Sigma Chemical Co., St. Louis, MO. PNP from rat erythrocyte was partially purified according to a published method.[13] With inosine as substrate, PNP activity was determined spectrophotometrically by a xanthine oxidase coupled assay.[14] The increase in absorbance at 293 nm was monitored with a Beckman DU-7 spectrophotometer. The typical assay contained 0.1 M HEPES/NaOH buffer, pH 7.4, 0.04 unit of xanthine oxidase (Boehringer Mannheim GmbH, West Germany), 1 mM (or 50 mM) sodium phosphate, appropriate concentrations of inosine (Sigma), and PNP in a total volume of 1.0 mL at 37 °C. Under these conditions, in the presence of 50 mM sodium phosphate, the specific activities of the four PNP, expressed as micromoles per minute per milligram of protein, were found to be 44 (human erythrocytes), 3.5 (rat erythrocytes), 116 (calf spleen), and 24 (*E. coli*).

Inhibition of PNP was measured at five concentrations of inosine and six concentrations of inhibitor. K_i values were determined by using a Dixon plot and a computer program developed in-house for linear regression analysis. It was determined that the inhibitors do not affect xanthine oxidase activity in the assay. For pH dependence studies, a three-component buffer system was used instead of HEPES. This buffer system[15] consisted of 0.052 M MES, 0.051 M TAPSO, 0.1 M diethanolamine, and HCl. The ionic strength of this mixture was 0.1 ± 0.01 M between pH 6.0 and 8.9.[15]

Registry No. **2**, 104495-32-1; **3**, 130434-88-7; **4**, 1478-53-1; **5**, 130434-89-8; **6**, 130434-90-1; **7**, 130434-91-2; **8**, 130434-92-3; PNP, 9030-21-1; $I(CH_2)_4I$, 628-21-7; $I(CH_2)_6I$, 629-09-4; 2-amino-6-chloropurine, 10310-21-1.

(13) Stoeckler, J. D.; Agarwal, R. P.; Agarwal, K. C.; Parks, R. E., Jr. *Methods Enzymol.* **1978**, *51*, 530–538.
(14) Kalckar, H. M. *J. Biol. Chem.* **1947**, *167*, 429–443.
(15) Ellis, K. J.; Morrison, J. F. *Methods Enzymol.* **1982**, *87*, 405–426.

Analysis of the Structures, Infrared Spectra, and Raman Spectra for the Methyl, Ethyl, Isopropyl, and *tert*-Butyl Radicals

J. Pacansky,* W. Koch,† and M. D. Miller

Contribution from the IBM Almaden Research Center, 650 Harry Road, San Jose, California 95120-6099. *Received May 7, 1990*

Abstract: Extensive ab initio calculations are reported for the optimized geometries of the methyl, ethyl, isopropyl, and *tert*-butyl radicals. In addition, vibrational frequencies and infrared and Raman intensities are computed and compared with experimental infrared spectra of the series of radicals. The theoretical calculations are used to assign experimental vibrational spectra and elucidate the radical structure.

Introduction

Alkyl radicals are perhaps the simplest but yet some of the most reactive organic radicals. They play a central role in the petroleum industry[1] and are reactive intermediates in the production of many commercial polymers.[2] As reactive intermediates they also play essential roles in polymer degradation,[3] thus determining the stability of many materials such as coatings and lubricants toward heat, light, and high-energy radiation.

Alkyl radicals thus have been the focus of active research in many industrial and academic laboratories. Studies have ranged from gas-phase kinetics for bond fission processes,[4] spectroscopic

† Present address: IBM Heidelberg Scientific Center, Institute for Supercomputing and Applied Mathematics, Tiergartenstrasse 15, D-6900 Heidelberg, West Germany.

(1) Leathard, D. A.; Purnell, J. H. Paraffin Pyrolysis. In *Annual Reviews of Physical Chemistry*, Eyring, H., Christensen, C. J., Johnston, H. S., Eds.; Annual Reviews: Palo Alto, CA, 1970; p 197.
(2) Hoyle, C. E., Kinstle, J. F., Eds. *Radiation Curing of Polymeric Materials*; ACS Symp. Ser. 417; American Chemical Society: Washington, DC, 1989.
(3) Schnabel, W. *Polymer Degradation: Principles and Practical Applications*; Macmillan Publishing Company, Inc.: New York, 1981.

0002-7863/91/1513-317$02.50/0

Table I. Comparison of Calculated Optimized Geometries for the Methyl, Ethyl, Isopropyl, and *tert*-Butyl Radicals (Bond Lengths, Å)

methyl		ethyl		isopropyl		*tert*-butyl	
C1H11	1.079	C1H11	1.082	C1H11	1.085	C2H21	1.102
		C2H21	1.099	C2H21	1.101	C2H22	1.094
		C2H22	1.093	C2H22	1.095	C2H23	1.094
		C1C2	1.492	C2H23	1.093	C1C2	1.493
				C1C2	1.493		

analysis,[5] chemical reactivity,[6] and theoretical calculations.[7] At the foundation of these studies are the series of radicals methyl (CH_3), ethyl (CH_3CH_2), isopropyl ($(CH_3)_2CH$), and *tert*-butyl ($(CH_3)_3C$) because they are the prototypes for primary, secondary, and tertiary radical centers from which a wealth of knowledge is gained about reactivity of unpaired electrons on the ends and along larger hydrocarbon chains, e.g., polymers. An important aspect of these studies is to determine the structure of the series of radicals to form a sound basis for kinetic studies. Third law calculations[8] are typically used to compute entropies which in turn require knowledge about symmetry, barriers for internal rotation, and other parameters leading to low-energy vibrational frequencies. Vibrational frequencies lower than $\simeq 500$ cm^{-1} increase entropy values, and prior knowledge of such effects is desirable.

In the past we have generated infrared spectra of alkyl free radicals[9] and have shown that they posses rather low frequency vibrations and that they have very low barriers[10] for internal rotation about the CC bonds attached to the carbon atom containing the unpaired electron; these bonds are generally referred to as α bonds; we will also loosely refer to the carbon atom with the unpaired electron as the radical site. A combined series of experiments and ab initio calculations have led to some structure elucidation.[11] Here, we augment these studies with extensive ab initio calculations on the structure, vibrational frequencies, infrared intensities, and Raman intensities on the series of radicals from methyl to *tert*-butyl. The calculations thus provide a consistent set of optimized geometries and vibrational spectra for this set of radicals, and they are compared with our experimental infrared spectra obtained for each in low-temperature matrices.[9]

Computational Details

Standard ab initio calculations were performed with the vectorized IBM version of Gaussian 86.[12] Several leads of theory were used; initial calculations were performed by using restricted open shell (ROHF) theory and a split valence 4-31G basis set; in addition, extensive unrestricted Hartree–Fock (UHF) calculations were performed by using the larger and more flexible 6-31G* and 6-311G** basis sets, which include polarization functions on carbon and on hydrogen as well as carbon, respectively. Finally, electron correlation effects were accounted for by 2nd order Moller–Plesset perturbation theory using the 6-311G** basis set.[12] For all cases, the geometry was optimized in D_{3h} (methyl), C_s (ethyl, isopropyl) and C_{3v} (*tert*-butyl) symmetry with use of analytical gradient methods. At the optimized geometries the force constants, harmonic frequencies, and infrared intensities were determined by analytical differentiation of the SCF wave functions and by numerically differentiating the analytical first derivatives of the UHF/MP2 energies. The Raman intensities were computed analytically at the UHF/6-311G** level for the methyl, ethyl, and isopropyl radicals and at the UHF/6-31G* level for the *tert*-butyl radical.

(4) Russell, J. J.; Seetula, J. A.; Timonen, R. S.; Gutman, D.; Nava, D. F. *J. Am. Chem. Soc.* **1988**, *110*, 3084. McMillen, D. F.; Golden, D. M. *Annu. Rev. Phys. Chem.* **1982**, *33*, 493.

(5) Wendt, H. R.; Hunziker, H. E. *J. Chem. Phys.* **1984**, *81*, 717. Chettur, G.; Snelson, A. *J. Phys. Chem.* **1987**, *91*, 5873.

(6) Rüchardt, C.; Beckhaus, H. D. *Top. Curr. Chem.* **1986**, *130*, 1. Rüchardt, C.; Beckhaus, H. D. *Angew. Chem.* **1985**, *97*, 531. Rüchardt, C.; Beckhaus, H. D. *Angew. Chem., Int. Ed. Engl.* **1985**, *24*, 529.

(7) Pacansky, J.; Yoshimine, M. *J. Phys. Chem.* **1985**, *89*, 1880. Pacansky, J.; Liu, B.; Defrees, D. *J. Org. Chem.* **1986**, *51*, 3720. Honjou, N.; Yoshinime, M.; Pacansky, J. *J. Phys. Chem.* **1987**, *91*, 4455. Schubert, W.; Yoshimine, M.; Pacansky, J. *J. Phys. Chem.* **1981**, *85*, 1340.

(8) Gutman, D. *Acc. Chem. Res.* In press. Benson, S. W. *Thermochemical Kinetics*, 2nd ed.; John Wiley and Sons: New York, 1976.

(9) (a) Pacansky, J.; Bargon, J. *J. Am. Chem. Soc.* **1975**, *97*, 6896. (b) Pacansky, J.; Dupuis, M. *J. Am. Chem. Soc.* **1982**, *104*, 415. (c) Pacansky, J.; Coufal, H. *J. Chem. Phys.* **1980**, *72*, 3298. (d) Pacansky, J.; Chang, J. S. *J. Chem. Phys.* **1981**, *74*, 5539.

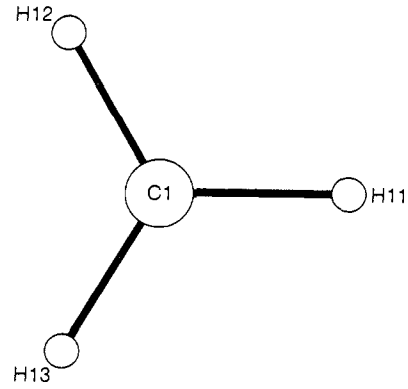

Figure 1. Structure of the methyl radical and atom labels used to specify the molecular geometry.

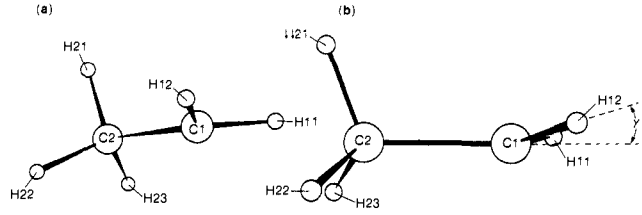

Figure 2. (a) Structure of the ethyl radical and atom labels used to specify the molecular geometry; (b) definition of γ, the pyramidal angle.

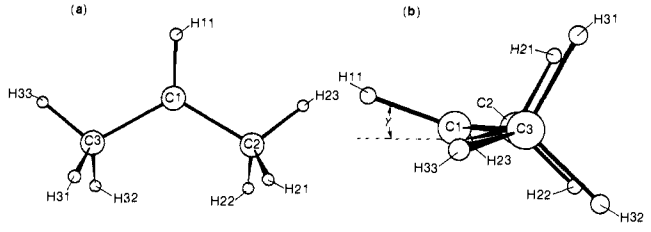

Figure 3. (a) Structure of the isopropyl radical and atom labels used to specify the molecular geometry; (b) definition of γ, the pyramidal angle.

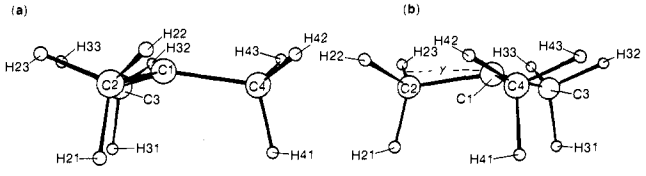

Figure 4. Structure of the *tert*-butyl radical and atom labels used to specify the molecular geometry; (b) definition of γ, the pyramidal angle.

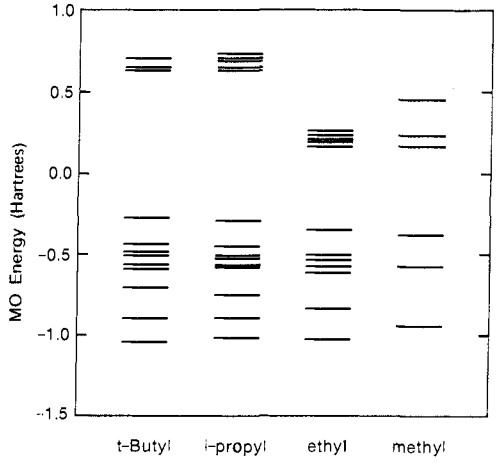

Figure 5. Pertinent molecular orbital energy level diagram for the methyl, ethyl, isopropyl, and *tert*-butyl radicals.

Table II. Comparison of Calculated Optimized Geometries for the Methyl, Ethyl, Isopropyl, and *tert*-Butyl Radicals (Bond Angles, deg)

	methyl		ethyl		isopropyl		*tert*-butyl	
	H11C1H12	120.0	H11C1H12	117.6	C2C1C3	119.8	C2C1C3	118.0
			H11C1C2	120.5	H11C1C2	118.4	C1C2H21	111.5
			C1C2H21	111.7	C1C2H21	111.5	C1C2H22	111.4
			C1C2H22	111.4	C1C2H22	110.9	C1C2H23	111.4
			H21C2H22	107.0	C1C2H23	111.9	H21C2H22	107.0
			H22C2H23	108.2	H21C2H22	106.7	H21C2H23	107.0
					H21C2H23	107.3	H22C2H23	108.3
					H22C2H23	108.3		
γ	0.0		11.9		18.6		24.1	

Table III. Calculated Harmonic and Observed Vibrational Frequencies (cm^{-1}) for CH_3

symmetry	mode	description	calcd ROHF/4-31G	calcd UHF/6-311G**	calcd UMP2/6-311G**	obsd ref 9a
E′	ν_1	deg. of CH stretch	3466.5	3407.4	3372.4	3162
	ν_2	deg. of CH_3 in-plane bend	1554.5	1512.4	1446.6	1396
A_1'	ν_3	sym CH_3 stretch	3281.0	3274.4	3179.4	
A_2'	ν_4	CH_3 out-of-plane bend	286.7	375.4	424.3	617

Table IV. Calculated Harmonic and Observed Vibrational Frequencies (cm^{-1}) for the Ethyl Radical C_2H_5 (C_s)

symmetry	mode	description	calcd ROHF/4-31G	calcd UHF/6-311G**	calcd UMP2/6-311G**	obsd ref 9b
A′	ν_1	sym αCH_2 stretch	3310	3264.3	3213.9	3033
	ν_2	asym CH_3 stretch	3212	3186.9	3129.3	2920
	ν_3	sym CH_3 stretch (βCH stretch)	3151	3119.6	3044.8	2842
	ν_4	CH_2 scissors	1651	1600.4	1511.0	
	ν_5	CH_3 bend	1616	1580.1	1496.0	
	ν_6	CH_3 umbrella	1586	1520.9	1421.7	1366
	ν_7	C-C stretch	1124	1101.6	1094.4	1138
	ν_8	CH_3 rock/CH_2 pyramidal bend	1100	1066.6	999.9	
	ν_9	CH_2 pyramidal bend	465	462.5	458.4	540
A″	ν_{10}	asym αCH_2 stretch	3414	3364.9	3325.1	3112
	ν_{11}	asym CH_3 stretch	3244	3221.4	3174.6	2987
	ν_{12}	CH_3 bend	1656	1603.3	1509.8	1440
	ν_{13}	CH_2/CH_3 wag	1334	1290.9	1218.4	1175
	ν_{14}	CH_3/CH_2 wag	901	860.9	820.9	
	ν_{15}	CH_2 torsion	160	163.8	160.8	

Table V. Calculated Harmonic and Observed Vibrational Frequencies (cm^{-1}) for the Isopropyl Radical C_3H_7 (C_s)

symmetry	mode	description	calcd ROHF/4-31G	calcd UHF/6-311G**	calcd UMP2/6-311G**	obsd Ref.9c
A′	ν_1	αCH stretch	3326	3284.8	3233	3069
	ν_2	deg. of CH_3 stretch	3242	3218.9	3168	2920
	ν_3	asym CH_3 stretch	3202	3178.1	3112	
	ν_4	sym CH_3 stretch (βCH stretch)	3142	3108.6	3029	2830
	ν_5	asym CH_3 bend	1659	1607.3	1514	1468
	ν_6	asym CH_3 bend	1654	1603.1	1503	1468
	ν_7	CH_3 umbrella	1592	1535.1	1429	1378
	ν_8	CH_3 wag	1313	1271.1	1198	
	ν_9	CH_3 rock	1168	1126.0	1058	
	ν_{10}	sym C–C–C stretch	929	920.2	910	
	ν_{11}	HC_3 pyramidal bend	478	470.2	439	369
	ν_{12}	C–C–C bend	384	374.6	362	
	ν_{13}	torsion	160	167.1	163	
A″	ν_{14}	asym CH_3 stretch	3242	3219.6	3169	2920
	ν_{15}	asym CH_3 stretch	3198	3174.3	3113	
	ν_{16}	sym CH_3 stretch (βCH stretch)	3138	3103.7	3027	2830
	ν_{17}	asym CH_3 bend	1649	1598.7	1503	1468
	ν_{18}	asym CH_3 bend	1643	1591.4	1492	1468
	ν_{19}	CH_3 umbrella	1578	1535.3	1439	1388
	ν_{20}	asym HC_3 bend (αCH wag)	1511	1467.5	1384	
	ν_{21}	asym C–C–C stretch	1219	1197.7	1178	
	ν_{22}	CH_3 rock	1064	1018.9	949	
	ν_{23}	CH_3 wag	1050	1006.5	947	
	ν_{24}	torsion	128	127	115	

Results

For all of the unrestricted calculations performed spin contamination of the UHF wave function was negligible. The expectation value for the spin eigenfunction when rounded off to two significant figures was equal to the correct value of 0.75. This is in line with past studies which have shown that UHF calculations are very reliable for alkyl radicals.[7]

In Tables I and II the results are listed for the optimized geometries using the extensive UHF MP2/6-311G** calculations.

Table VI. Calculated Harmonic and Observed Vibrational Frequencies (cm^{-1}) for the *tert*-Butyl Radical C_4H_9 (C_s)

symmetry	mode	description	calcd ROHF/4-31G	calcd UHF/6-31G*	calcd UMP2/6-31G*	obsd ref 9d
E	ν_1	asym CH_3 stretch	3244.4	3262.0	3186.6	
	ν_2	asym CH_3 stretch	3203.5	3220.2	3136.3	2931
	ν_3	sym CH_3 stretch (βCH stretch)	3130.7	3137.7	3038.2	2825
	ν_4	asym CH_3 bend	1659.5	1640.5	1562.0	1455
	ν_5	asym CH_3 bend	1643.6	1623.1	1538.8	
	ν_6	CH_3 umbrella	1573.7	1554.1	1462.1	1371
	ν_7	CH_3 wag	1406.4	1394.3	1351.3	1229
	ν_8	CH_3 rock	1102.6	1088.3	1050.5	
	ν_9	asym CC stretch	1049.4	1026.9	973.7	811
	ν_{10}	asym CCC bend	407.4	397.2	387.8	541(?)
	ν_{11}	CH_3 torsion	156.8	158.1	164.7	
A_1	ν_{12}	asym CH_3 stretch	3209.6	3226.8	3136.9	2931
	ν_{13}	sym CH_3 stretch (βCH stretch)	3138.2	3146.5	3043.3	2825
	ν_{14}	asym CH_3 bend	1661.9	1642.5	1557.1	1455
	ν_{15}	CH_3 umbrella	1597.7	1577.3	1484.5	1367
	ν_{16}	CH_3 rock	1234.7	1206.5	1156.5	992
	ν_{17}	sym CC stretch	795.5	799.9	792.8	733
	ν_{18}	sym CCC bend (pyramidal bend)	296.6	288.1	281.8	
A_2	ν_{19}	asym CH_3 stretch	3236.5	3254.5	3182.6	
	ν_{20}	asym CH_3 bend	1640.9	1620.5	1540.0	
	ν_{21}	sym CH_3 wag	1084.5	1055.8	1001.4	
	ν_{22}	sym CH_3 torsion	144.5	143.1	163.9	

Table VII. Calculated Infrared and Raman Intensities for CH_3

			infrared intensity, km/mol		raman UHF/6-311G**	
symmetry	mode	description	UHF/6-311G**	UMP2/6-311G**	intensity	depol
E′	ν_1	deg. of asym CH stretch	11.0	4.13	36.5	0.75
	ν_2	deg. of asym in-plane bend	2.23	3.03	1.87	0.75
A_1'	ν_3	sym CH stretch	0.00	0.00	134.0	0.13
A_2'	ν_4	out-of-plane bending	80.3	82.74	0.00	

Table VIII. Calculated Infrared and Raman Intensities for the Ethyl Radical C_2H_5

			infrared intensity, km/mol		raman UHF/6-311G**	
symmetry	mode	description	UHF/6-311G**	UMP2/6-311G**	intensity	depol
A′	ν_1	sym αCH_2 stretch	18.9	14.14	113.7	0.139
	ν_2	asym CH_3 stretch	42.3	21.59	91.7	0.332
	ν_3	sym CH_3 stretch (βCH stretch)	41.6	22.21	133.9	0.117
	ν_4	CH_2 scissors	4.23	1.82	11.6	0.738
	ν_5	CH_3 bend	1.52	4.62	3.98	0.75
	ν_6	CH_3 umbrella	0.268	1.65	1.45	0.722
	ν_7	C–C stretch	0.031	0.04	6.99	0.298
	ν_8	CH_3 rock/CH_2 pyramidal bend	0.0849	0.24	3.46	0.358
	ν_9	CH_2 pyramidal bend	47.8	52.18	2.99	0.574
A″	ν_{10}	asym αCH_2	27.8	13.21	48.1	0.75
	ν_{11}	asym CH_3 stretch	38.0	18.97	86.6	0.75
	ν_{12}	CH_3 bend	4.35	5.24	11.3	0.75
	ν_{13}	CH_2/CH_3 wag	1.82	1.96	1.22	0.75
	ν_{14}	CH_3/CH_2 wag	1.03	1.70	0.022	0.75
	ν_{15}	CH_2 torsion	0.451	0.26	2.87	0.75

Table I contains the results for the bond lengths while Table II displays the computed results for the relevant bond angles. Figures 1–4 contain drawings illustrating the numbering scheme used to describe the geometrical parameters; these figures also provide a definition for the out-of-plane bending angle, γ, for the ethyl, isopropyl, and *tert*-butyl radicals.

The molecular orbital energy levels computed are listed in Figure 5 for each radical while Figure 6 contains orbital plots for the HOMO of each radical.

The computed vibrational frequencies, along with the available experimental values, are listed in Tables III–VI for the methyl, ethyl, isopropyl, and *tert*-butyl radicals, respectively; the computed infrared and Raman intensities are contained in Tables VII–X. The reliability of computed infrared and Raman spectra has been extensively studied in the past few years and is well-documented in the literature.[14] In general, computed harmonic frequencies tend to overestimate the experimental, anharmonic frequencies. This is due to the combined effect of (i) the neglect of anharmonicity and (ii) the insufficiency of the theoretical method. The

(10) (a) Pacansky, J.; Coufal, H. *J. Chem. Phys.* **1980**, *72*, 5285. (b) Pacansky, J.; Yoshimine, M. *J. Phys. Chem.* **1987**, *91*, 1024. (c) Pacansky, J.; Yoshimine, M. *J. Phys. Chem.* **1986**, *90*, 1980.

(11) Pacansky, J.; Schrader, B. *J. Chem. Phys.* **1983**, *78*, 1033. Schrader, B.; Pacansky, J.; Pfeiffer, U. *J. Phys. Chem.* **1984**, *88*, 4069.

(12) Frisch, M. J.; Binkley, J. S.; Schlegel, H. B.; Raghavachari, K.; Melius, C. F.; Martin, R. L.; Stewart, J. J. P.; Bobrowicz, F. W.; Rohlfing, C. M.; Kahn, L. R.; DeFrees, D. J.; Seeger, R.; Whiteside, R. A.; Fox, D. J.; Fluder, E. M.; Pople, J. A. *Carnegie*-Mellon Quantum Chemistry Publishing Unit: Pittsburgh, PA, 1984.

(13) Hehre, W.; Radom, L.; Schleyer, P. v. R.; Pople, J. A. *Ab initio Molecular Orbital Theory*; Wiley Interscience: New York, NY, 1986; Chapter 4.

(14) Yamaguchi, Y.; Frisch, M.; Gaw, J.; Schaefer, H. F.; Binkley, J. S. *J. Chem. Phys.* **1986**, *84*, 2263.

Table IX. Calculated Infrared and Raman Intensities for C_3H_7

			infrared intensity, km/mol		raman UHF/6-311G**	
symmetry	mode	description	UHF/6-311G**	UMP2/6-311G**	intensity	depol
A′	ν_1	αCH stretch	49.6	27.36	90.90	0.207
	ν_2	asym CH_3 stretch	35.3	18.54	103.2	0.690
	ν_3	asym CH_3 stretch	73.4	44.66	161.0	0.251
	ν_4	sym CH_3 stretch (βCH stretch)	65.9	33.26	240.2	0.089
	ν_5	sym CH_3 deg. bend	4.35	4.74	17.31	0.749
	ν_6	asym CH_3 bend	12.8	15.22	2.400	0.671
	ν_7	CH_3 umbrella	3.04	4.96	1.597	0.727
	ν_8	CH_3 wag	2.04	2.04	1.229	0.285
	ν_9	CH_3 rock	0.364	0.14	0.732	0.214
	ν_{10}	sym C–C–C stretch	1.75	1.75	8.142	0.252
	ν_{11}	HC_3 pyramidal bend/torsion	17.9	20.73	3.098	0.501
	ν_{12}	out of plane wag/C–C–C scissors	3.76	4.56	0.4528	0.617
	ν_{13}	torsion	0.158	0.12	0.5177	0.725
A″	ν_{14}	asym deg. of CH_3 stretch	39.2	19.26	72.50	0.75
	ν_{15}	asym CH_3 stretch	11.2	4.98	22.46	0.75
	ν_{16}	sym CH_3 stretch (βCH stretch)	29.7	25.47	20.71	0.75
	ν_{17}	asym CH_3 bend	0.663	0.45	6.894	0.75
	ν_{18}	asym CH_3 bend	1.32	1.99	16.96	0.75
	ν_{19}	CH_3 umbrella	5.26	10.28	3.476	0.75
	ν_{20}	HC_3 bend (αCH wag)	4.65	1.52	0.4438	0.75
	ν_{21}	asym C–C–C stretch	0.048	0.04	4.454	0.75
	ν_{22}	CH_3 rock	0.171	0.43	2.926	0.75
	ν_{23}	CH_3 wag	0.427	0.70	0.2083	0.75
	ν_{24}	torsion	0.001	0.01	0.1618	0.75

Table X. Calculated Infrared and Raman Intensities for the *tert*-Butyl Radical C_4H_9

			infrared intensity, km/mol		raman UHF/6-31G*	
symmetry	mode	description	UHF/6-31G*	UMP2/6-31G*	intensity	depol
E	ν_1	asym CH_3 stretch	71.8	36.36	112.9	0.75
	ν_2	asym CH_3 stretch	20.6	10.22	34.08	0.75
	ν_3	sym CH_3 stretch (βCH stretch)	30.5	25.83	19.76	0.75
	ν_4	asym CH_3 bend	2.29	3.14	22.27	0.75
	ν_5	asym CH_3 deg. of bend	1.85	3.08	22.78	0.75
	ν_6	CH_3 umbrella	2.19	6.77	5.135	0.75
	ν_7	sym CH_3 wag	5.24	4.75	1.112	0.75
	ν_8	deg. of CH_3 rock	1.59	2.32	7.189	0.75
	ν_9	asym C–C stretch	0.024	0.17	5.326	0.75
	ν_{10}	asym C–C–C bend	0.108	0.04	0.1129	0.75
	ν_{11}	CH_3 torsion	0.0198	0.00	0.3071	0.75
A_1	ν_{12}	asym CH_3 stretch	70.4	47.12	184.7	0.142
	ν_{13}	sym. CH_3 stretch (βCH stretch)	82.2	37.84	259.4	0.084
	ν_{14}	asym CH_3 bend	13.2	19.01	5.401	0.739
	ν_{15}	CH_3 umbrella	1.39	1.81	4.244	0.538
	ν_{16}	CH_3 rock	0.516	0.00	0.734	0.000
	ν_{17}	sym C–C stretch	0.942	0.98	8.731	0.113
	ν_{18}	sym C–C–C bend (pyramidal bend)	2.57	3.66	0.0829	0.405
A_2	ν_{19}	asym CH_3 stretch	0.00	0.00	0.00	0.75
	ν_{20}	asym CH_3 bend	0.00	0.00	0.00	0.75
	ν_{21}	sym CH_3 wag	0.00	0.00	0.00	0.75
	ν_{22}	sym CH_3 torsion	0.00	0.00	0.00	0.75

extent of this overestimation depends on the chosen 1-particle basis set and to which extent electron correlation has been taken into account. Hartree–Fock SCF calculations employing small, split valence type basis sets like 4-31G usually lead to an overestimation of the computed frequencies of about 10–12%. The use of polarized split or triple valence basis sets, like 6-31G* or 6-311G**, does not significantly improve the accuracy of the computed spectrum, whereas the inclusion of electron correlation effects through 2nd order Moller–Plesset perturbation theory typically reduces this error to 5–6% at MP2/6-31G* and MP2/6-311G**, the best theoretical level used in this study. To achieve an even better agreement very large basis sets including f-type polarization functions have to be employed.[15] Very often, a uniform scaling factor is applied to the theoretical frequencies to achieve better agreement with the experimental spectrum. It should, however, be noted that such a uniform scaling of all frequencies with only one scaling factor may even deteriorate the agreement with the experimental frequencies for some modes. Known examples are multiple bond stretching and out-of-plane deformation modes for which the computed unscaled frequencies are sometimes even smaller than the experimental frequencies (see below).[16] The theoretically predicted IR intensities are usually in qualitative agreement (order and approximate ratio of intensities) with the experimental spectrum when theoretical levels like HF/6-31G* are used, while smaller basis sets are known to give unreliable results. The inclusion of electron correlation effects through MP2 yields improved intensities, although much higher levels of theory using large basis sets and a better treatment of electron correlation are needed for accurate results.[17,18]

(15) Simandiras, E. D.; Rice, J. E.; Lee, T. J.; Amos, R. D.; Handy, N. C. *J. Chem. Phys.* **1988**, *88*, 3187.

(16) Pacansky, J.; Wahlgren, U.; Bagus, P. S. *Theor. Chim. Acta (Berlin)* **1976**, *41*, 301.

(17) Bagus, U. I.; Pacansky, J.; Bagus, P. S. *J. Chem. Phys., J. Chem. Phys.* **1975**, *63*, 2874.

(18) Bagus, P. S.; Pacansky, J.; Wahlgren, U. *J. Chem. Phys.* **1977**, *67*, 618.

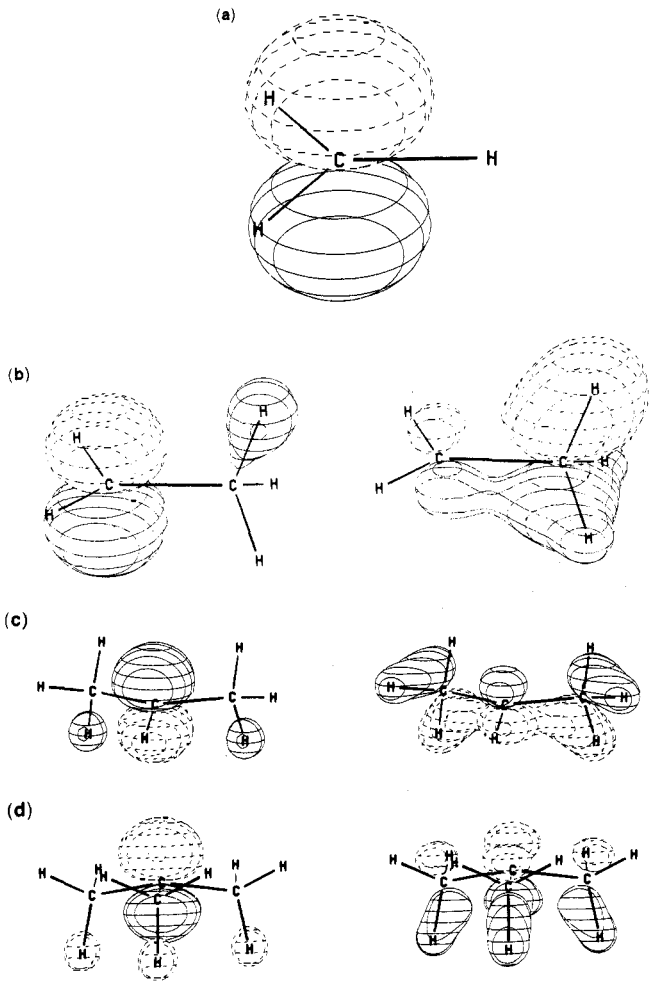

Figure 6. (a) The HOMO orbital plot for the methyl radical; the two molecular orbitals involved in a hyperconjugative effect in (b) the ethyl radical, (c) the isopropyl radical, and (d) the *tert*-butyl radical.

The thrust of the present study is to provide insight for the structure of alkyl radicals. Thus, vibrational modes characteristic of primary, secondary, and tertiary radical centers are illustrated in Figure 7, while the experimental infrared spectra for the methyl, ethyl, isopropyl, and *tert*-butyl radicals are shown in Figure 8. For the sake of providing a direct experimental-to-theoretical comparison we also show the computed infrared and Raman spectra in Figures 9 and 10; here, the spectra are presented using a Lorentizian function for each band shape; the same width was used for each band. Figures 11–14 contain computer drawings for the characteristic vibrational modes.

Discussion

Geometry. The results for the geometry optimization for the methyl, ethyl, isopropyl, and *tert*-butyl systems are summarized in Tables I and II and shown in Figures 1–4. These indicate that the methyl radical is planar with a D_{3h} symmetry. This result has been obtained with extensive SCF ROHF calculations[19] and was the conclusion of a gas-phase microwave study.[20] The ethyl, isopropyl, and *tert*-butyl radicals have nonplanar radical centers with overall C_s symmetry for the ethyl and isopropyl radicals and a C_{3v} symmetry for the *tert*-butyl radical. The only symmetry element found for the ethyl radical is a single plane that bisects the ethyl radical with the CC bond lying in the plane. For the isopropyl radical the plane of symmetry contains the lone αCH bond with the two methyl groups lying symmetrically opposed to the plane. The nonplanar geometry about the radical center introduces some "s" character into the carbon p orbital containing

(19) Pacansky, J. *J. Phys. Chem.* **1982**, *86*, 485.
(20) Hirota, E. *J. Phys. Chem.* **1983**, *87*, 3375.

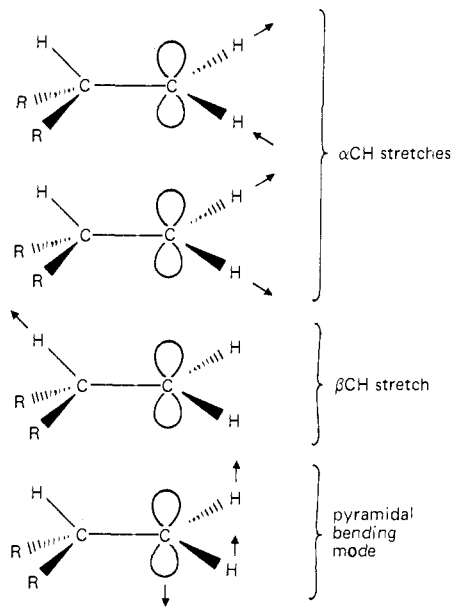

Figure 7. An illustration for the characteristic vibrational modes for primary alkyl radicals; the diagram is easily extended to secondary and tertiary radicals by merely replacing αH with say methyl groups.

the unpaired electron so that the geometry acquires a pyrimadal structure resembling ammonia. Thus, for example, the ethyl radical structure is similar to that of ethane where now a βCH bond is trans to the unpaired electron; the isopropyl radical has two βCH bonds, and the *tert*-butyl radical has three βCH bonds located trans to the unpaired electron.

Closer examination of each optimized geometry indicates that, when appropriate, each system has shorter than normal bonds α to the radical center with methyl groups that have a slight tilt away from the radical site. Within each methyl group we find that the CH bonds trans to the p orbital containing the unpaired electron are longer than the CH bonds in a gauche position.

The degree of non-planarity of the radical sites is given by γ which is defined in Figures 2–4, respectively. γ, which is of course zero for the methyl radical, changes considerably with methyl substitution.

The αCH bond length in CH_3 is $r_{\alpha CH}$ = 1.079 Å, which is shorter than those for sp^3 bond lengths, e.g., in C_3H_6, r_{CH} = 1.093 Å (obtained via MP2/6-311G** calculations) and slightly shorter than that found for sp^2 CH bond lengths, e.g., in C_2H_4, where r_{CH} = 1.085 Å (obtained via MP2/6-311G** calculations). There is a slight increase in the αCH bond length with methyl substitution from the methyl radical to the *tert*-butyl radical. The interesting feature here is that the αCH bond length lengthens with methyl substitution but for isopropyl the length is the same as for the sp^2 CH bond length in ethylene.

The αCC bond lengths, $r_{\alpha CC}$ = 1.492 Å, like the αCH bond lengths, are shorter than normal CC single bond lengths, for example, in ethane, r_{CC} = 1.527 Å, but considerably longer than C=C bond lengths, e.g., for ethylene, $r_{C=C}$ = 1.336 Å. However, they appear to change very little with methyl substitution.

The βCH bond lengths in the methyl groups are slightly longer than 1.09 Å and have about the same length as those found in ethane where r_{CH} = 1.093 Å. An interesting feature of the methyl group geometry, which as shown below has a profound effect on vibrational spectra, is that the βCH bonds are not equivalent. Those trans to the unpaired electron are longer than those in a gauche position. In fact the two gauche βCH bonds in the isopropyl radical are in nonequivalent positions and hence have slightly different bond lengths; the gauche CH bonds in the tertiary butyl radical are symmetrically equivalent and hence have equal bond lengths.

We should add that the optimized geomtries for the UHF MP2/6-311G** calculations display similar trends using smaller basis sets or ROHF calculations with larger basis sets.

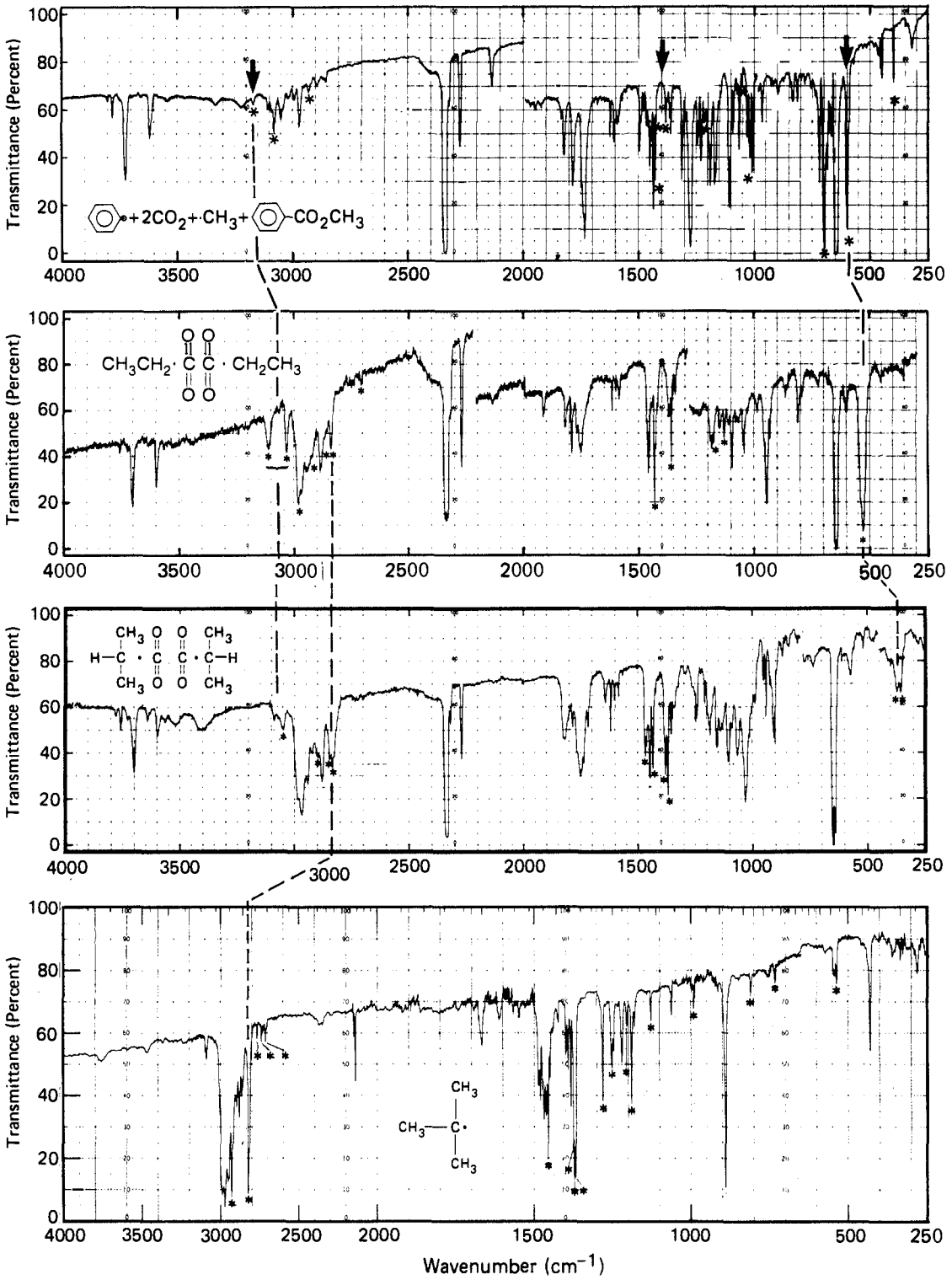

Figure 8. Infrared spectra for the methyl radical (top), the ethyl radical, the isopropyl radical, and the *tert*-butyl radical (bottom), isolated in rare gas matrices.

Ionization Potentials. Consider the energy levels for all of the molecular orbitals shown in Figure 5. The HOMO has the lowest energy for the methyl radical but increases with methyl substitution, thus, in the order from the methyl to the *tert*-butyl radical, the HOMO energies are 10.5, 9.59, 8.04, and 7.56 eV, which on the basis of Koopmans' theorem is equal to the ionization potential for each system. Experimental values[21] for the ionization potential are 9.85, 8.50, 7.69, and 6.92 eV. Thus, the UHF MP2/6-311G** calculations yield vertical ionization potentials close to the experimental values also showing a decrease with methyl substitution; this effect may be explained on the basis of an inductive effect whereby the methyl groups donate charge to the radical center. The calculation of ionization potentials was also investigated in detail by Liu and co-workers.[22]

Hyperconjugation: Homo Orbital Plots. The origin of the nonequivalent βCH bonds was investigated by obtaining orbital plots for the HOMOs of each radical. The HOMO orbital plots are given in Figure 6. The orbital plot for the methyl radical in

(21) Houle, F. A.; Beauchamp, J. L. *J. Am. Chem. Soc.* **1979**, *101*, 4067.

(22) Lengsfield, B. H., III; Siegbahn, P. E. M.; Liu, B. *J. Chem. Phys.* **1984**, *81*, 710.

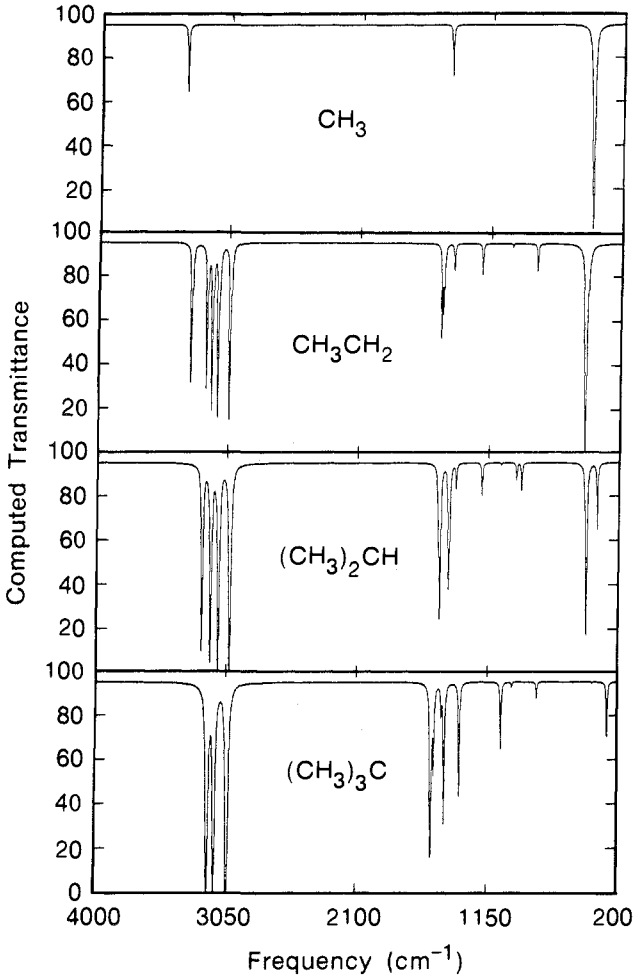

Figure 9. Computed infrared spectra for the methyl, ethyl, isopropyl, and *tert*-butyl radicals (see Computational Details).

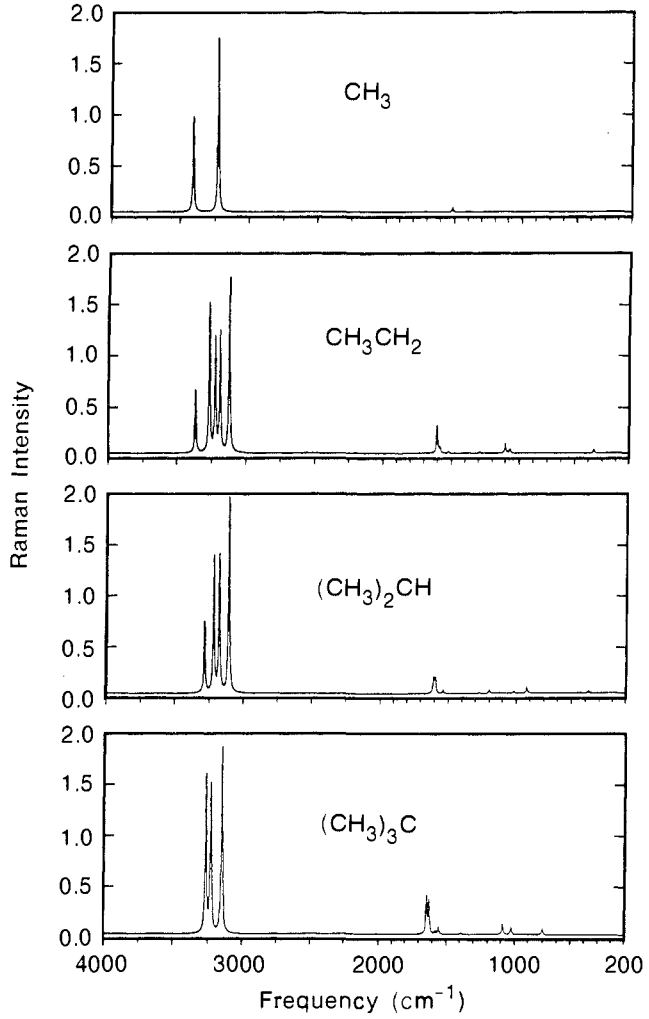

Figure 10. Computed Raman spectra for the methyl, ethyl, isopropyl, and *tert*-butyl radicals (see Computational Details).

Figure 6a shows clearly that the unpaired electron resides in a p orbital on the carbon atom. A different picture is obtained for the ethyl radical shown in Figure 6b where now in addition to the C 2p orbital the HOMO also contains a large contribution from a βCH bond that is eclipsed with the C 2p orbital and geometrically located in a trans position. The HOMO orbital plots for the isopropyl and *tert*-butyl radicals contained in Figure 6, parts c and d, also consist of contributions from the C 2p orbital containing the unpaired electron and βCH bonds eclipsed with the radical center, with the exception that instead of one bond, now two and three βCH bonds are involved, respectively.

The nonequivalent βCH bonds as well as the shortening of the αCC bonds compared to regular CC single bonds are the consequence of hyperconjugative interaction[23] between the formally singly occupied p-orbital at the radical center and the molecular orbital for the eclipsed βCH bond. Orbital plots for the two relevant molecular orbitals (the singly occupied and a doubly occupied MO) are shown in Figure 6, b–d. In all cases (with the obvious exception of CH_3) the αCC bond adopts a partial double bond character while the electron density in the βCH bonds eclipsed to the αC 2p orbital is decreased, thus weakening, i.e., lengthening, these bonds.

Vibrational Frequencies and Intensities. The computed vibrational frequencies, along with the available experimental values, are listed in Tables III–VI for the methyl, ethyl, isopropyl, and *tert*-butyl radicals, respectively; the computed infrared and Raman intensities are contained in Tables VII–X. A few generalizations are pertinent; first vibrational frequencies computed at the SCF level have values that are consistently too high but the computed order (that is, for example, from high to low frequencies) has been very dependable. Hence, in order for a clearer comparison between experiment and theory most authors multiply the computed frequencies by a scaling factor. This is not done here merely because

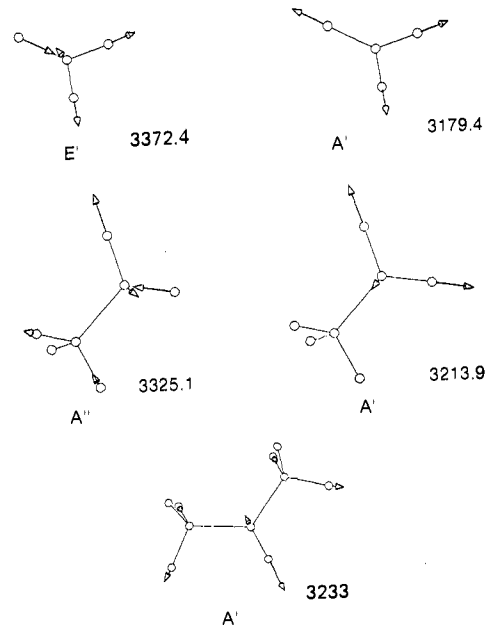

Figure 11. Normal mode displacement diagrams for the αCH stretches for the methyl, ethyl, and isopropyl radicals.

(23) Dewar, M. J. S. *J. Am. Chem. Soc.* **1984**, *106*, 669. Mulliken, R. S.; Rieke, C. A.; Brown, W. G. *J. Am. Chem. Soc.* **1941**, *63*, 41.

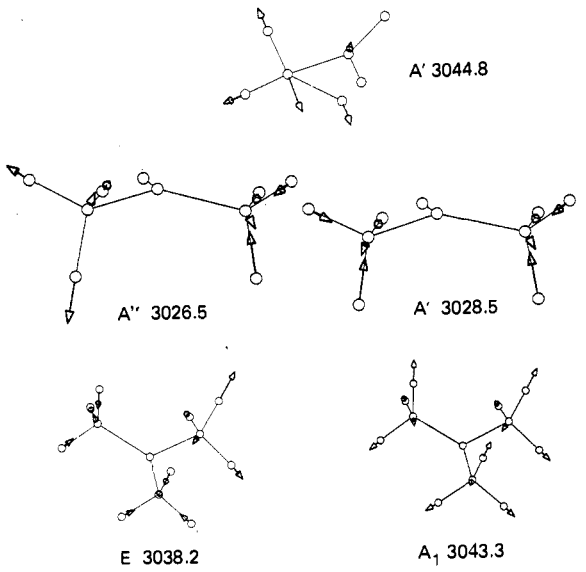

Figure 12. Normal mode displacement diagrams for the βCH stretches for the ethyl, isopropyl, and *tert*-butyl radicals.

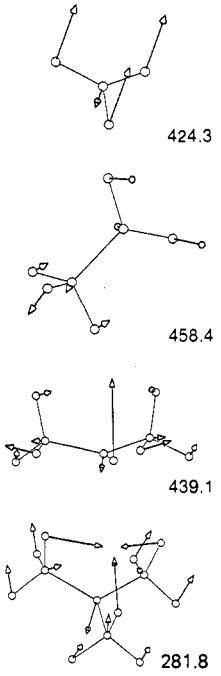

Figure 13. Normal mode displacement diagrams for the pyramidal bending frequency for the methyl, ethyl, isopropyl, and *tert*-butyl radicals.

we are comparing vibrational modes for four systems and do not want to generate more numbers than necessary. Second, although SCF theory gives us frequencies that are too high as clearly seen by examination of the results for the 4-31G and 6-311G** calculations, adding correlation to the calculation decreases the frequencies making them closer to experimental values.

The optimized geometry for the methyl radical has a D_{3h} symmetry which dictates that the IR modes are Raman inactive and the Raman modes are IR inactive and that two degenerate vibrational modes have E′ symmetry, one has A_1' symmetry, and another has A_2'. The two E′ modes are described as degenerate asymmetric C–H stretches and in-plane H–C–H bends; the A_1' mode is a symmetric C–H stretch while the A_2' mode is best described as an out-of-plane bending mode of the radical center. The A_2' mode has been referred to as an umbrella or pyramidal bending motion similar to the mode responsible for the inversion of NH_3. This description applies for ethyl, isopropyl, and *tert*-butyl radicals where the radical center is nonplanar but not strictly for the methyl radical because of its planar geometry; nevertheless,

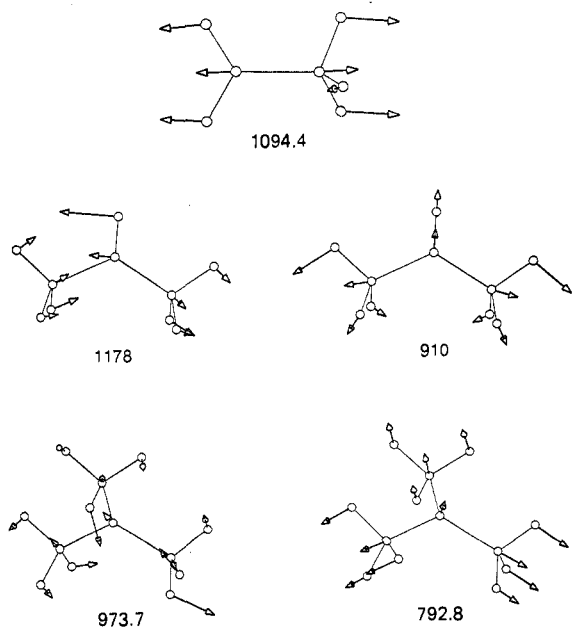

Figure 14. Normal mode displacement diagrams for the CC stretches in the ethyl, isopropyl, and *tert*-butyl radicals.

in order to discuss the trend from methyl to *tert*-butyl radical we will also loosely refer to the mode as an umbrella, etc., mode.

As shown in Table III the computed frequencies at the highest level of theory are about 6% too high for the C–H stretches and about 5% too high for the in-plane bends; this excellent trend does not carry out for the A_2'' out-of-plane bending which is about 30% lower than experiment. This discrepancy is not completely unexpected as the potential energy surface for the out-of-plane bend is very flat. It has been shown that for some systems the inclusion of higher angular momentum functions is important for the computation of symmetric bends, particularly at the correlated level.[15] The effects of higher angular momentum polarization functions were examined for the methyl radical with a TZ2P(f) basis and were found to raise the frequency by only 12%. Thus, in this instance anharmonicity is likely the major feature influencing the computed frequency.

The C_s symmetry of the ethyl radical dictates that the 15 vibrational modes separate into 9 with A′ symmetry and 6 with A″ symmetry and that all of the modes are Raman and infrared active. The vibrational frequencies follow the same trend found for the ethyl radical as noted above for the methyl radical, that is the smaller 4-31G basis at the SCF level gives frequencies about 9–10% too high, for the larger 6-311G** basis the agreement with experiment is closer and is the closest for the MP2/6-311G** computation ($\simeq$6% too high) which includes some correlation. This trend continues for the lower frequency mode, and the agreement with experiment is somewhat better for the umbrella bending motion of the radical center which is now only $\simeq$15% too high. The assignment of the modes follows the experimental assignment for the CH stretching frequencies where enough experimental data seem to be available. In addition the experimental assignment of the frequency at 540 cm^{-1} is without doubt the umbrella mode of the radical center; theory agrees with this assignment. Although several other vibrational frequencies were experimentally observed their assignment is not certain and in this context theory is very important.

The two highest frequencies for the ethyl radical, at 3325.1 and 3213.9 cm^{-1}, are assigned to the A″ asymmetric and A′ symmetric stretching frequencies of the methylene group; these frequencies are in nominal range for CH stretches of carbon in an sp^2 electronic configuration.

The CH stretching frequencies associated with the methyl group in the ethyl radical are computed at 3174.6, 3129.3 and 3044.8 cm^{-1}. The A′ and A″ asymmetric stretches are usually degenerate; the slight splitting computed here reflects the distortion of the geometry from a C_{3v} local symmetry. The A′ symmetric CH_3

stretch, at 3044.8 cm^{-1}, is an important vibrational mode and is discussed at length below.

The frequencies for the valence angle bending for the methylene group and the methyl group are computed to be 1511.0 (A′), 1509.8 (A″), 1496.0 (A′), and 1421.7 (A′) cm^{-1}. The vibrational mode responsible for the 1511.0 cm^{-1} is best described as a scissor-like bending motion of the methylene group. The frequencies at 1509.8 and 1496.0 cm^{-1} are asymmetric bending motions of the H–C–H bond angles in the methyl group; in alkanes, these frequencies are degenerate or approach degeneracy as the bond angles and lengths in the methyl group (and the H–C–C angles) become equivalent. The 1421.7-cm^{-1} frequency is attributed to the symmetric bending motion H–C–H in the methyl groups.

The vibrations in the lower frequency range that is the rocking and wagging motion of the methyl group, the wagging and umbrella motion of the methylene group, and the C–C stretch require additional introductory comments. First, we define a methyl rock as a motion where the changes in the H–C–C angles, H22C2C1 and H23C2C1, have the same sign (see Figure 2) or the motion where the methyl group moves toward or away from the methylene group while retaining the C_s symmetry; conversely, the wagging motion is not symmetric to the plane and hence the changes in the H22C2C1, H23C2C1 angles have opposite signs. The umbrella motion of the methylene group has the same local symmetry as the methyl rocking; the wagging motion is antisymmetric to the plane of symmetry. One further comment is that all rocking, wagging, and umbrella modes and the C–C stretching motion are considerably mixed, and in some cases it is difficult to decide which description is best. This is consistently encountered for most low-frequency vibrations, and certainly the systems studied in this report display the same trends. With these comments in mind the 1094.4-cm^{-1} (A′) band is the C–C stretch, the 999.9-cm^{-1} (A′) band is a methyl rocking motion, the 458.4-cm^{-1} (A′) band is the umbrella motion of the methylene group, the 1218.4-cm^{-1} (A″) band is a methylene wagging, the 820.9-cm^{-1} (A″) band is a methyl wagging, and the 160.8-cm^{-1} (A″) band is the torsional motion of the methyl and methylene groups about the C–C bond.

We should add that the assignment for the 1218.4 and 999.9 cm^{-1} to a methyl or methylene wag is most difficult. The 1218.4-cm^{-1} mode contains some C–C stretch which tends to increase the frequency and make the assignment difficult. Previously[9] the reverse assignment was chosen, but on the basis of the present results we tend to favor the assignment herein (see the theoretical work on the ethyl dication by Wong et al.[24] for additional details on the ethyl radical).

Of the series of alkyl radicals from ethyl, to isopropyl, to *tert*-butyl, the isopropyl system fits the trend the least. This radical has C_s symmetry with the plane of symmetry containing the αCH bond; the radical center is nonplanar and all of the bond angles and bond lengths in and around a methyl group are nonequivalent. This is clearly seen upon inspection of Figure 4 and Tables I and II. Note that due to the rotation of the methyl groups out of the CCC plane all of the CH bonds are nonequivalent; the manifestation of this subtle change in geometry on vibrational frequencies is a splitting of otherwise degenerate vibrations (a theoretical study on the isopropyl radical by Chen et al.[25] has recently appeared, and it is in accord with the present results).

The frequency at 3233 cm^{-1} is the stretching mode of the αCH bond. The asymmetric stretching motions (here we mean local symmetry of one methyl group) of the C–H bonds in the methyl groups are around 3168 and 3113 cm^{-1} while the symmetric stretches are around 3027 cm^{-1}. Due to the C_s symmetry the CH_3 stretches for both methyl groups must be symmetric and antisymmetric to the plane of symmetry. Hence, the calculated frequencies occur in nearly degenerate pairs, that is, computed asymmetric CH_3 frequencies are found at 3169 (A″) and 3168 (A′) cm^{-1} and at 3113 (A″) and 3112 (A′) cm^{-1}; the symmetric CH_3 stretches are at 3029 (A′) and 3037 cm^{-1}. The fact that the frequencies for vibrations only differing by the point group symmetry are so close indicated that very little coupling occurs between the methyl groups.

The H–C–H bending frequencies within a methyl group may also be described in terms of local symmetry as asymmetric and symmetric bending motions which in terms of the point group symmetry will occur in pairs symmetric and antisymmetric to the plane of symmetry. Thus, the asymmetric CH_3 bends are at 1514 (A′) and 1503 (A″) cm^{-1} and at 1503 and 1492 cm^{-1}; the symmetric bends are at 1439 (A″) and 1429 (A′) cm^{-1}. The A″ motions are not pure CH_3 bending modes, but due to symmetry they contain some contribution from the bending of the H11–C1–C2 and H11–C1–C3 angles.

The vibrations in the lower frequency range of the isopropyl radical are mixtures of modes that occur in this region, and as before we will attempt to give the best description for each. The asymmetric bending motion of the H11–C1–C2 angles (or the wagging of the αCH bond) is at 1384 cm^{-1}. This mode is mixed with the wagging of the methyl groups and is similar to ν_{13} of the ethyl radical where this mode is a mixture of a CH_3, CH_2 wag and a small amount of C–C stretch.

It is instructional to compare the rocking and wagging modes of the isopropyl radical with those of the ethyl radical. Since each methyl group has one rocking and wagging motion then the two methyl groups in the isopropyl have two rocks and wags that are linear combinations related by the plane of symmetry. In the ethyl radical the wagging mode, ν_{14} is 820.9 cm^{-1}; in the isopropyl system the A′ is at 1198 cm^{-1} while the A″ is at 947 cm^{-1}. Thus, for the A′ wag where the two methyl groups move toward each other, the frequency increases significantly from the case where we have only one methyl (i.e., ethyl radical) group while when the methyl groups move away from each other, as they do for the A″ motion, the frequency is considerably lower but closer to that for the ethyl radical.

The rocking motion of a methyl group in the ethyl radical maintains the plane of symmetry via a tilting motion toward the CH_2 group and has a frequency at 999.9 cm^{-1}. For the isopropyl radical the A′ mode is at 1058 cm^{-1} while the A″ mode is at 949 cm^{-1}. Thus, the A′ rocking motion of two methyl groups has a higher frequency because the two methyl groups move in phase toward the radical center; the methyl groups move out of phase during the A″ motion and hence they interact less resulting in a lower frequency. Since the A′ and A″ motions are still directed toward the radical center and not at each other then the smaller changes in the frequencies are reasonable.

The symmetric and asymmetric C–C–C stretching frequencies are at 1178 and 910 cm^{-1}. The C–C–C bending motion is at 362 cm^{-1}.

The pyramidal bending of the radical center is computed to be at 439 cm^{-1} and will be discussed in more detail below. The torsion motions are at 163 and 115 cm^{-1}.

The 33 vibrational frequencies for the *tert*-butyl radical, according to its C_{3v} point group symmetry, are separated into 22 vibrations of E symmetry species therefore forming 11 E type modes, 7 of A_1 and 4 of A_2 symmetry; the E and A_1 vibrations are IR and Raman active while the A_2 vibrations are optically inactive.

The local vibrational modes of the methyl groups dominate the spectrum of the *tert*-butyl radical. The vibrations associated with the three methyl groups are the following: nine C–H stretches of which three are degenerate asymmetric stretches of E symmetry and three are nondegenerate, two of A_1 and one of A_2 symmetry; nine H–C–H valence angle bends, of which three are degenerate asymmetric stretches of E symmetry and three are nondegenerate, two of A_1 and one of A_2 symmetry; three rocking modes, one with E symmetry and one with A_1 symmetry; and three wagging motions of which one has E and one has A_2 symmetry.

The carbon skeleton connecting the methyl groups to the radical center contributes three C–C–C stretching motions, one with E symmetry and one with A_1 symmetry, and three C–C–C angle

(24) Wong, M. W.; Baker, J.; Nobes, R. H.; Radom, L. *J. Am. Chem. Soc.* **1987**, *109*, 2245.
(25) Chen, Y.; Rauk, A.; Tschuikow-Roux, T. *J. Phys. Chem.* **1990**, *94*, 2775.

bending modes, one degenerate with E symmetry and one with A_1 symmetry.

The last set of vibrations include the three torsional motions, two of which are degenerate and have E symmetry while the last one is optically inactive with A_2 symmetry.

The vibrational frequencies with E type symmetry, calculated at 3186.6, 3136.3, and 3038.2 cm^{-1}, are, in terms of local symmetry, the degenerate asymmetric and symmetric stretching motions of the C–H bonds in the methyl groups. According to the local symmetry of a methyl group only the asymmetric stretch is degenerate; the symmetric stretch is degenerate because of the C_{3v} point group symmetry. The frequencies at 3136.9 and 3043.3 cm^{-1} are assigned to the A_1 stretches, which again with local CH_3 symmetry are asymmetric and symmetric stretches, and the 3182.6-cm^{-1} vibration is assigned to the A_2 asymmetric stretch. The frequencies at 3038.2 and 3043.3 cm^{-1} are βCH stretching motions, have high intensities, and dominate experimental IR spectra of the *tert*-butyl radical.

The H–C–H valence angle bending motions of the methyl groups, unlike the ethyl and isopropyl radicals, appear to be nearly pure vibrational motions. The computed frequencies at 1562.0 and 1538.8 cm^{-1} are assigned to the asymmetric bends; the 1462.1-cm^{-1} frequency is assigned to the symmetric bend. The frequencies at 1557.1 and 1484.5 cm^{-1} are assigned as the A_1 asymmetric and symmetric bends while the frequency at 1540.0 cm^{-1} is attributed to the A_2 asymmetric bend.

The wagging motions are calculated to be at 1351.3 and 1001.4 cm^{-1} for the degenerate E type mode and the A_2 mode. The trend in the wagging frequencies from the ethyl system to the *tert*-butyl system follows a trend toward higher frequency as the number of methyl groups in the system increases; this most likely is a reflection of the increase in steric crowding with methyl substitution. For the ethyl system the wag is at 820.9 cm^{-1} and the two wags for the isopropyl system are at 1198 and 947 cm^{-1}, while for the *tert*-butyl system the E and A_2 type wags are at 1351.3 and 1001.4 cm^{-1}. Since the wagging motions in the *tert*-butyl radical force each methyl group out of the vertical symmetry planes bisecting each group, then for the E motions where all of the methyl groups move against each other we expect a higher frequency. The A_2 vibration is a motion whereby all methyl groups undergo a wagging motion in the same direction, i.e., in phase, and the result is a substantial lowering of the frequency for this mode.

The rocking motions of the methyl groups are computed to be at 1050.5, and 1156.5 cm^{-1} for the E and A_1 modes, respectively. Comparison of these with the rocking motions of ethyl and isopropyl shows a trend. For example, the A′ mode in ethyl, the A′ mode for isopropyl, and the A_1 mode for *tert*-butyl all involve rocking in-phase motions of the methyl toward the radical center. The frequencies 999, 1058, and 1156.5 cm^{-1} in the order ethyl to *tert*-butyl, respectively, increase as the number of methyl groups around the radical center increases. Thus the energy that is required to rock methyl groups toward the radical center increases with the number of CH_3 groups.

The vibrational modes of the carbon skeleton are computed to be at 973.7 cm^{-1} for the E type asymmetric C–C stretches and at 792.8 cm^{-1} for the symmetric C–C stretch. The bending modes are calculated to be at 387.8 cm^{-1} for the degenerate asymmetric bends and 281.8 cm^{-1} for the A_1 symmetric bending.

The torsional motions are computed at 164.7 cm^{-1} for the degenerate E mode and at 163.9 cm^{-1} for the inactive A_2 mode.

The infrared spectrum of an alkyl radical consists of two parts: those modes which are a manifestation of the radical site and other modes quite similar in character to the closed-shell parent hydrocarbon. Viewed in this perspective, the respective radical center (i.e., a primary, secondary, or tertiary radical site) gives rise to infrared and Raman absorptions in specific regions much like other organic functional groups, such as ketones, C=C double bonds, etc. The ensuing discussion develops this line of thought through a comparison of experimental and theoretical vibrational spectra.

In all cases studied thus far, vibrational modes involving motions of the bonds α and β to the radical site differ from the spectra of closed-shell hydrocarbons. Bonds more distant from the radical site appear to be affected little and hence the vibrational motions for this part of the radical are quite similar to the spectrum of the closed-shell parent hydrocarbon. The specific vibrational motions involving the α and β bonds are the stretching modes of the αCH and αCC bonds, the stretching motions of the βCH and βCC bonds, and the pyramidal-like bending motion of the radical center. The characteristic vibrational motions are illustrated in Figure 7.

Consider the experimental infrared spectra in Figure 8 which will be used to point out the characteristic modes. There, the absorptions assigned to the respective radical are labeled. First, the infrared spectrum of the methyl radical contains a band with a very weak intensity (relative to the very intense band at 607 cm^{-1} due to the out-of-plane bending mode of the radical center) at 3171 cm^{-1}, assigned to the doubly degenerate asymmetric αCH stretch. As shown in Figure 8, substitution of one of the α hydrogens of the methyl radical to form the ethyl radical gives rise to two relatively intense absorptions at 3122 and 3032 cm^{-1} due to the asymmetric and symmetric stretches of the αCH bonds in the ethyl radical. Further substitution of one of the α hydrogens in the ethyl radical produces the isopropyl system whose vibrational spectrum now contains a band at 3064 cm^{-1} attributed to the stretching motion of the lone αCH bond. Substitution of all of the α hydrogens with methyl groups forms the *tert*-butyl radical, and of course absorptions are not observed at frequencies higher than 3000 cm^{-1}, as shown in Figure 8.

The theoretical infrared and Raman spectra for the series of radicals are shown in Figures 9 and 10. In particular, the theoretical spectra for modes assigned to the αCH stretches (already delineated in the tables) closely parallel the experimental spectra. The nature of the motion involving each αCH stretch is described in Figure 11 by plotting the atomic displacements for each normal mode obtained from the theoretical analysis.

While substitution of methyl groups for α hydrogens produces a change in the infrared spectrum above 3000 cm^{-1}, concomitantly, new bands assigned to stretching motion of the βCH bonds are observed from 2840 to 2800 cm^{-1}. It is pertinent to note that the vibrational spectra of organic systems containing only carbon and hydrogen are devoid of absorptions in this spectral region. As shown in Figure 8 only one band at 2840 cm^{-1} is observed for the ethyl radical, two bands at 2850 and 2830 cm^{-1} are observed for the isopropyl system, the band at higher frequency has a much lower intensity, and the magnitude of the observed splitting is larger than theoretically predicted; the origin for this is not known. For the *tert*-butyl radical only one band at 2825 cm^{-1} is detected. Here, theory predicts absorptions for two bands that are accidentally degenerate in this region. Since only one band is observed, agreement is found between theory and experiment. Again, the theoretical infrared spectra for the systems under study in the βCH stretching region are an excellent reproduction of the experimental spectrum. The atomic displacements described by each mode are shown in Figure 12; all involve a stretching motion of a βCH bond with a slightly longer bond length that, in the case of ethyl and *tert*-butyl radicals, is eclipsed with the half-filled p orbital containing the unpaired electron. The βCH bond with the longest bond length in the isopropyl is not exactly eclipsed with the half-filled p orbital on the radical center, but the motion is almost identical. In all systems, there is a contribution to the motion from other βCH bonds, but a study on the partially deuterated system,[10a] HCD_2CD_2, gave a βCH stretching frequency that was identical with the βCH frequency for CH_3CH_2; clearly, on this basis there can be at best weak coupling with other vibration modes in the system qualifying this as a characteristic frequency for a radical site.

The experimental spectra contained in Figure 8 and the theoretical spectra illustrated in Figures 9 and 10 show that βCH bond stretching frequencies have rather high IR intensities (see also Tables VII–X). This is also true for Raman bands and will be most useful for studies in this area.

Perhaps the most interesting characteristic mode for an alkyl radical is the pyramidal bending motion of the radical center. The

pyramidal bending frequency is observed at 605 cm^{-1} for the methyl radical, at 540 cm^{-1} for the ethyl radical, and at 382 and 366 cm^{-1} for the isopropyl radical. No bands could be assigned in the low-frequency part of the IR spectra to the *tert*-butyl radical in the spectrum shown in Figure 8. This spectral feature has a very strong intensity marked by a rather large natural bandwidth (see Figure 8). It overwhelms the IR spectrum of the methyl radical, dominates the ethyl radical IR spectrum, certainly is one of the more intense bands in the isopropyl radical spectrum, but is too weak to be detected, as yet, in the spectrum of the *tert*-butyl radical. Again, the theoretical IR spectrum closely matches the intensity and band centers of the observed spectrum. The theoretical spectra reproduce the experimental spectra excellently for all of the systems. The only objectionable feature that may be an issue is the intensity, and maybe the band center for the pyramidal bending mode of the tertiary butyl system. Considering the absorption for the βCH stretching mode of the *tert*-butyl system shown in Figure 8, and the intensity of the theoretical βCH stretching mode relative to intensity of the pyramidal bending mode, we should have experimentally observed this band if in fact it did have a band center above 200 cm^{-1}. Consequently, either theory may be predicting too high an intensity for a bending mode of this sort where only CCC bonds are involved or the computed band center is off. If the latter situation exists, that is the experimental frequency is less than 200 cm^{-1}, then it would be outside of the detection of the IR experiments. This is certainly a possibility considering that the motion is very anharmonic and involves a large amplitude. That a slight problem may exist is obtained by comparing intensities of the methyl and ethyl radicals, where the agreement of relative intensities of βCH to pyramidal bending is excellent, with those for the isopropyl and *tert*-butyl systems, where the agreement is still good for the isopropyl but fair for the *tert*-butyl radical. From this we conclude that the theory is apparently predicting intensities for pyramidal bending modes involving CH bonds differently from those involving more CC bonds.

The absorptions associated with the CC bond stretches have not been experimentally identified with any degree of certitude. They are an important set of vibrations that should provide direct information about αCC and βCC bonds. Presently, it is believed that, like other IR absorptions associated with CC bonds, they have a very low intensity and are also coupled to other vibrational modes. Hence, the band centers are variable making them difficult to identify. Here, the theoretical results are important because of their predictive power providing insight for designing experiments. The computed CC stretching vibrations for each system are described in Figure 14. The CC stretch for the ethyl radical, 1094 cm^{-1}, is higher than that found for normal CC single bonds; of course, this follows for the result of theory because, as listed in the tables, all αCC bonds are shorter than expected as a result of the increases in sp^2 character introduced by the unpaired electron. Addition of a methyl group, to form the isopropyl system, gives rise to two bands centered at 1178 and 910 cm^{-1}; these are the asymmetric and symmetric stretching frequencies. The CC stretching frequencies for the *tert*-butyl system are computed to be at 973.7 cm^{-1} (E symmetry) for the asymmetric stretch and 800 cm^{-1} (A_1) for the symmetric stretch. The infrared intensity of the CC stretch in the ethyl radical is very weak on an absolute scale, and for example on a scale relative to the low-frequency βCH stretch it is $\simeq 1/500$ the intensity. Although this does not improve for the other systems, absolute intensities for the symmetric CC stretches are about a factor of 4 larger than those for the asymmetric stretches. The situation improves slightly in the Raman where the intensities are not the lowest but still a substantial improvement. Here, for the ethyl radical, the intensity ratio for the CC stretch/βCH $\simeq 1/19$; slightly smaller ratios are found for the other systems. In view of the experimental problems encountered to produce alkyl free radicals in large quantities to detect weak, but important absorptions, theory predicts that this endeavor has more merits when Raman scattering techniques are used.

Concluding Remarks and Summary

A knowledge of the structure of small alkyl radicals is of wide-spread importance in the areas of gas-phase kinetics, thermodynamics, and theory of chemical bonding. The series of alkyl radicals from the methyl to the *tert*-butyl play a central role in these studies because they are the simplest systems on which a large number of studies have been performed. Consequently, we have reported an exhaustive set of calculations on the methyl, ethyl, isopropyl, and *tert*-butyl radicals to obtain a consistent structural analysis. In addition, the vibrational frequencies and infrared and Raman intensities have also been calculated and compared to experimentally observed IR spectra. The fact that excellent agreement is found between the theoretical and observed IR spectra provides credence for the ab initio radical structures and furthermore provides an incentive for conducting Raman experiments of the radicals in low-temperature matrices.